IEEE Access
Multidisciplinary | Rapid Review | Open Access Journal

Received 6 October 2023, accepted 30 October 2023, date of publication 6 November 2023, date of current version 9 November 2023.

Digital Object Identifier 10.1109/ACCESS.2023.3330237

RESEARCH ARTICLE

A Flexible Virtual Inertia and Damping Control Strategy for Virtual Synchronous Generator for Effective Utilization of Energy Storage

PRATEEK UTKARSHA, (Graduate Student Member, IEEE), N. K. SWAMI NAIDU, BATTA SIVAPRASAD, AND KUMAR ABHISHEK SINGH

Department of Electrical Engineering, Indian Institute of Technology (BHU) Varanasi, Varanasi, Uttar Pradesh 221005, India

Corresponding author: Prateek Utkarsha (prateekutkarsha.rs.eee18@iitbhu.ac.in)

This work was supported by the Science and Engineering Research Board-Department of Science and Technology (SERB-DST) India under Grant ECR/2018/001214.

ABSTRACT This paper presents a flexible virtual inertia and damping control strategy for a virtual synchronous generator (VSG) for the effective utilization of energy storage. Due to their low inertia and low kinetic energy, power electronics-based renewable energy sources are becoming more and more prevalent, which poses major dependability issues for the grid. However, the typical synchronous generator has the ability to adjust to changes in the grid frequency and voltage thanks to load frequency management and an automatic voltage regulator. So, emulating the synchronous machine characteristics in the power electronics-based converter system increases the stability of the grid and further increases the renewable energy penetration in the grid. However, VSG power and frequency oscillates when a sudden disturbance in the power demand occurs in the distributed generation system. This article focuses on minimizing the frequency oscillations as well as power oscillations of VSG during transient conditions or disturbances. Initially, the impact of varying inertia and damping on the active power control loop of VSG is investigated. In addition, the parameters of the VSG are designed in order to minimize the requirement of discharge/charge from the energy storage. So, in this paper, a control strategy with flexible virtual inertia and damping coefficient is designed for optimizing the energy storage unit to support frequency stability. The proposed control method is verified in the developed experimental prototype. In addition, proposed control algorithm is compared with the currently available adaptive control approaches like adaptive inertia control (adaptive J control) and alternating inertia and damping (alternating J and D_P control) based VSG and observed that the energy storage requirement and the oscillations in the active power and frequency are minimum in the proposed control method as compared to the other two methods.

INDEX TERMS Damping coefficient, flexible virtual inertia, frequency stability, small signal modeling, virtual synchronous generator.

NOMENCLATURE

T_m	Reference torque.
T_e	Output electrical torque of VSG.
P_m	Reference active power.
P_e	Active power output of VSG.
θ	Virtual rotor angle.
ω	VSG frequency in rad/sec.
ω_0	Reference frequency in rad/sec.
E	Generated voltage reference.
D_P	Virtual damping of VSG.
J	Virtual inertia of VSG.
Q^*	Reference reactive power.
Q	Reactive power output of VSG.
k_{iq}	Integrator gain in reactive power loop.
D_q	Droop coeficient of the reactive power loop.
V_o^*	Output voltage reference.
V_o	VSG output voltage.

The associate editor coordinating the review of this manuscript and approving it for publication was Yuh-Shyan Hwang.

I. INTRODUCTION

In recent times, the inadequacy of conventional energy sources and the rising energy demand of fuels have made it necessary to include more unconventional/renewable energy sources (RES) that frequently use the interfacing converters for power generation. Non-conventional sources of energy, like solar, wind etc., contribute a significant part in enhancing the efficiency, stability and lowering the transmission losses when their penetration is lower compared to conventional synchronous generators [1]. However, the characteristics of conventional power systems change with increasing proportion of unreliable power electronics-based RES, which have neither mechanical rotors nor inertia [2]. Due to the increasing penetration of these RES, the total inertia of the power system decreases, and it affects the frequency stability during certain events [3].

The low inertia of power systems has an adverse effect on conventional power system stability. Firstly, lower inertia causes poor frequency response during the event of disturbances because the kinetic energy wouldn't be sufficient to keep the frequency at a certain level. Secondly, a significant drop in total inertia leads to a quick acceleration or deceleration of the system frequency, which causes to fail the safety mechanisms of the generating units [4]. Virtual synchronous generator (VSG) is presented in [5] and [6] to address the instability issues brought up by the insufficiency of inertia in power electronics-driven renewable systems. Similar to the droop control in microgrids [7], VSG replicates the features of an already existing synchronous generator to make sure that the electric grid operates efficiently and safely. Numerous models of the VSG exist in the literature [8]. One of the variants is the synchronverter [9], which adopts the phase-locked loop (PLL) for synchronization. Grid forming control is trending nowadays due to the microgrid advancement. Hence, a grid forming VSG with the improved PLL operation is presented in [10] for stable operation under transient conditions. Further, a self-synchronized VSG is presented in [11], which completely removes the PLL unit. A different approach is presented in [12] to mimic synchronous machines using voltage components called voltage-based virtual synchronous machines (VSM). A virtual flux orientation-based VSG is presented in [13] to decouple the active and reactive power. A VSM-based electric vehicle charger is presented in [14], which can supply households in the absence of a grid with the help of an electric vehicle battery. To get a better look into the design procedure of VSG parameters, such as inertia and damping, a small signal modeling of VSG is presented in [15]. All the above-mentioned VSG control methods work in voltage-controlled mode. However, a grid-forming vector current control scheme is presented in [16] to emulate the VSG characteristics in the existing current-controlled inverter systems. Nonetheless, the aforementioned VSG techniques have not addressed stability problems during transient conditions.

When the generation from renewable energy sources fluctuates significantly, the output power and frequency of the VSG may oscillate. A Number of control methods were put forth to lower the oscillatory output of real power and VSG frequency. An enhanced power decoupling method for VSG is presented in [17] to improve the stability. An integrator is introduced into the active power control loop [18] to enhance the transient stability of VSG under grid faults. In addition, to get better dynamic behavior, an optimal control method of VSG is presented in [19], considering the limitation of frequency acceleration (slope) and deviation in VSG frequency. In essence, the output characteristics can be changed directly by modifying the variables of VSG, i.e., inertia and damping, which affect the oscillations of power and frequency [20]. A novel approach to adaptive inertia control (adaptive J control) is presented in [21] by choosing different inertia values in different states. However, this strategy does not take the effect of the damping factor into consideration. An adaptive inertia-based fuzzy synchronverter is presented in [22]. But this scheme also doesn't consider the virtual damping effect in an active power loop. Adaptive damping control of VSG for damping out the frequency oscillation is presented in [23].

Inertia and damping choices affect the reliability of VSG as well as the cost-effectiveness of energy storage configurations. The virtual inertia of VSG helps in supporting the micro-grid frequency as well as VSG. But even though the optimum values of inertia and damping are used, those parameters are fixed throughout the operation of the VSG. Hence, automatically adjusting inertia and damping-based VSG is presented in [24] to suppress the frequency transients. When calculating the damping and inertial power as described in [24], the computational load on the digital signal processor is increased due to the usage of online optimization (DSP).

In [25], a new auto-tuned (AT)-VSG-based frequency control approach is presented to lessen the DSP's computational load. In [26], adaptive virtual inertia, as well as virtual damping control of VSG (alternating J and D_P control), is presented, in which alternating values of inertia and damping are used in different intervals. In addition, the size of the DC storage element and the cost of the system are greatly influenced by the choice of the damping parameter and inertia. Hence, the optimized design of the parameters of VSG will have an impact on the stability and storage capacity of the renewable energy system [27]. In [28] and [29], artificial neural network-based control of a virtual synchronous generator is presented. Parameters of VSG are predicted by training the neural network in [28] and [29], which is a complex process. In [30], an adaptive dynamic programming method for VSG is presented to suppress the power and frequency oscillations. A robust damping control strategy for VSG is presented in [31] to suppress the oscillations in active power during disturbances, but it doesn't reflect the inertia effect.

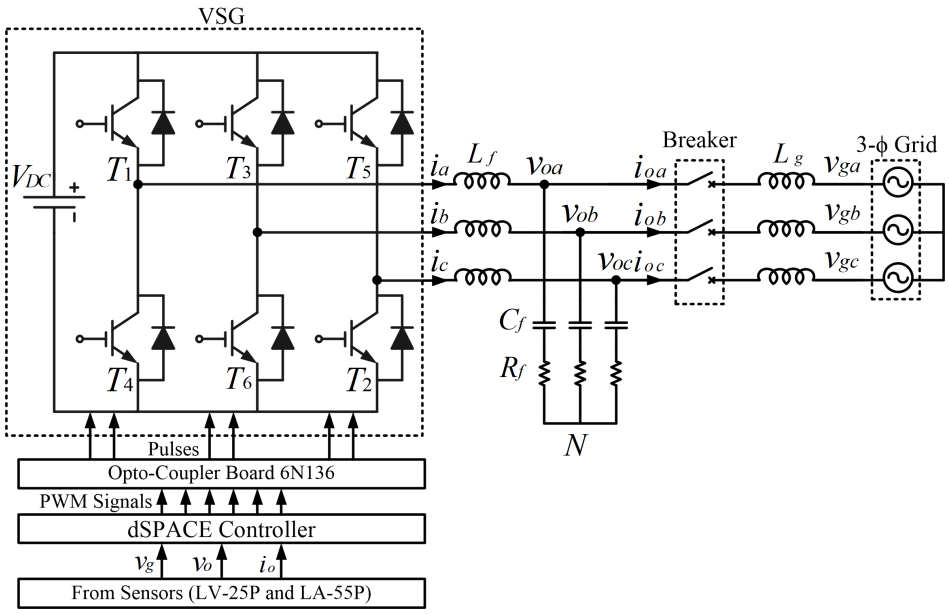

FIGURE 1. Schematic diagram of virtual synchronous generator.

One of the issues with the aforementioned adaptive control methods, such as adaptive inertia control, variable inertia as well as variable damping method, is that extreme values of both the VSG parameters have been chosen in different intervals, but there is no explanation for the effect on the other control loops because of the extreme values of inertia and damping. Also, there is no analysis found in the literature that considers the energy storage requirement for designing the parameters of VSG active power loop in the case of robust/adaptive control of virtual inertia and damping.

The contribution of this paper is to analyze the simultaneous adjustment of both damping and inertia for better transient characteristics of the power loop of VSG. The effect of parameters on the energy absorbed by the storage unit is analyzed in order to understand its consideration while designing the parameters. Later, A flexible inertia and damping-based control method is depicted to effectively utilize the energy storage system. Further, the proposed control algorithm is compared with the adaptive J control [21] and alternating J and D_P control [26] in terms of energy storage usage.

The rest of the article is organized as follows: The schematic and operating principle of the considered VSG is depicted in section II. A small signal representation of a virtual synchronous generator is presented in section III. Time domain analysis of VSG to find out the effect of parameter variation on active power and frequency is presented in Section IV. Energy absorbed/supplied by the storage unit with the fluctuation in active power is investigated in detail in section V. A flexible control method of virtual inertia and damping of VSG is proposed in section VI. This proposed control strategy is simulated in the MATLAB platform, and verified results are discussed in section VII. Experimental results of the VSG prototype are discussed in section VIII. The conclusion comes next in section IX.

II. BLOCK DIAGRAM REPRESENTATION

The schematic representation of the VSG structure is depicted in Fig. 1, where, v_o, i, i_o & L_f indicates the output voltage, inverter current, output current and filter inductance of the VSG respectively. L_g and v_g represents the grid interfacing inductance and grid voltage respectively. Filter resistance and capacitance are denoted by R_f and C_f respectively.

The control algorithm for VSG comprises the properties of synchronous generator such as kinetic inertia and damping. Thus, eqns. (1)-(3) can be used to express the VSG equations. Equations (1) and (2) reflect the VSG's active power loop, whereas equation (3) describes the reactive power loop.

$$T_m - T_e - D_P(\omega - \omega_0) = J\frac{d\omega}{dt} \tag{1}$$

$$\frac{P_m}{\omega_0} - \frac{P_e}{\omega} - D_P(\omega - \omega_0) = J\frac{d\omega}{dt} \tag{2}$$

$$\sqrt{2}E = k_{iq}\int (Q^* - Q) + \sqrt{2}D_q(V^*{}_o - V_o) \tag{3}$$

Here, D_P and J denotes the virtual damping and the virtual inertia respectively. Reference or mechanical torque of the VSG is T_m and torque generated by VSG is T_e. VSG rotor angle and angular velocity is denoted by θ and ω respectively. ω_0 is the reference frequency in rad/sec. Reference active power (P_m) and reference frequency (ω_0) are used to calculate reference torque (T_m). VSG output active power (P_e) and frequency (ω) are used to determine the generated electrical torque (T_e). Output voltage reference and actual output voltage are indicated by V_o^* and V_o respectively whereas E stands for the generated voltage reference. Output

reactive power and the reference reactive power of VSG are Q and Q^* respectively.

III. SMALL SIGNAL MODEL OF VSG

The active power control loop's small signal model is produced by equation (2) at the static operating points specified in equation (4). It is assumed that each state variable, x, has a value of X_n at static condition, with a minor disturbance, $\hat{x}$, i.e.

$$\omega_0 = \omega_{0n} + \hat{\omega_0}, \quad P_e = P_{en} + \hat{P}_e,$$
$$P_m = P_{mn} + \hat{P_m}, \quad \delta = \delta_n + \hat{\delta}, \quad \omega = \omega_n + \hat{\omega} \tag{4}$$

where, δ is the load angle. Assuming $\hat{\delta}$ is very small, $\sin\hat{\delta} \approx \hat{\delta}$. Since, ω_0 is nearly equal to steady state value, $\widehat{\omega_0} = 0$.

Applying small signal perturbation in equation (2), the small signal model of the active power controller will become as,

$$\frac{\widehat{\delta}(s)}{\hat{P}_m(s) - \hat{P}_e(s)} = \frac{1}{\left(J\omega_0 s + D_p\right)s} \tag{5}$$

Also small signal open loop transfer function of active power can be derived as:

$$\frac{\hat{P}_e(s)}{\widehat{\delta}(s)} = \frac{3V_{on}V_{gn}}{X_s} \tag{6}$$

Fig. 2 illustrates the small signal representation of active power loop of the VSG as shown below,

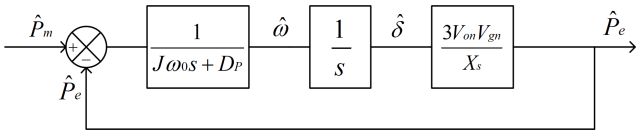

FIGURE 2. Small signal representation of VSG active power loop.

IV. TRANSIENT PERFORMANCE OF ACTIVE POWER LOOP OF VSG

This section presents the transient response analysis of VSG active power loop. Firstly, mathematical expression of step response of active power is given in section (A). Then, transient performance of VSG is analyzed with constant values of inertia and damping in (B). Later, transient performance of VSG with respect to variable virtual damping and inertia is analyzed in (C) & (D) respectively.

A. STEP RESPONSE OF ACTIVE POWER AND PARAMETERS

Active power to reference power transfer function is derived from Fig. 2 as,

$$\frac{\hat{P}_e}{\hat{P_m}} = \frac{\frac{K}{J\omega_0}}{s^2 + \frac{D_P}{J}s + \frac{K}{J\omega_0}} \tag{7}$$

And VSG frequency to reference power transfer function is derived as,

$$\frac{\hat{\omega}}{\hat{P_m}} = \frac{s}{s^2 + \frac{D_P}{J\omega_0}s + \frac{K}{J\omega_0}} \tag{8}$$

where, $K = \frac{3V_{on}V_{gn}}{X_s}$= constant

V_{on} and V_{gn} are nominal output voltage and grid voltage of VSG. X_s denotes the grid impedance. Now natural frequency of oscillation ω_N, damping ratio ζ and damping frequency ω_d of this second order system is given in equation (9) as,

$$\omega_N = \sqrt{\frac{K}{J\omega_0}} \text{ and } \zeta = \frac{D_P}{2}\sqrt{\frac{\omega_0}{JK}}$$
$$\omega_d = \frac{1}{2J}\sqrt{\frac{4JK - D_P^2\omega_0}{\omega_0}}$$
$$\phi = \cos^{-1}\zeta = \cos^{-1}\frac{D_P}{2}\sqrt{\frac{\omega_0}{JK}} \tag{9}$$

Therefore, the step response of active power with change in reference power is given in equation (10) as:

$$\hat{P}_e(t) = \hat{P_m}[1 - \frac{e^{-\zeta\omega_N t}}{\sqrt{(1-\zeta^2)}}sin(\omega_d t + \phi)] \tag{10}$$

Transient response parameters such as rise time (t_r), peak time (t_p), settling time (t_s) and peak overshoot (M_p) of this system can be given in equation (11a)-(11c) as follows,

$$t_r = 2J\sqrt{\frac{\omega_0}{4JK - D_P^2\omega_0}}(\pi - \phi) \tag{11a}$$

$$t_p = 2\pi J\sqrt{\frac{\omega_0}{4JK - D_P^2\omega_0}} \tag{11b}$$

$$t_s = \frac{8J}{D_P}, \quad M_p = e^{-\pi D_P}\sqrt{\frac{\omega_0}{4JK - D_P^2\omega_0}} \tag{11c}$$

B. VIRTUAL DAMPING'S IMPACT ON THE DYNAMIC PERFORMANCE OF VSG

Effect of virtual damping coefficient D_P on transient behaviour of active power can be analyzed, by finding the derivative of transient response parameters (t_p, t_s, M_p) with respect to D_P.

From equation (11), we can get the derivative of transient response parameter with respect to damping coefficient D_P as,

$$\frac{dt_p}{dD_P} > 0, \quad \frac{dt_s}{dD_P} < 0 \quad \& \quad \frac{dM_p}{dD_P} < 0 \tag{12}$$

We can see that peak time is increasing function with respect to D_P, hence the peak time increases with increasing damping coefficient. However, peak overshoot and settling time are decreasing function with respect to D_P. Hence, overshoot and settling time reduces with increasing damping coefficient. Effect of variation of damping on transient response of active power is shown in Fig. 3.

Similarly, influence of damping coefficient D_P on the VSG frequency can be analyzed using equation (8). Peak time, peak overshoot and settling time of frequency, all are decreasing with increasing D_P. Effect of variation of damping on frequency response of VSG is depicted in Fig. 4.

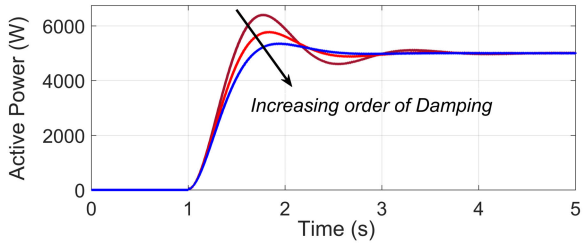

FIGURE 3. Active power response of VSG with variation in damping D_P.

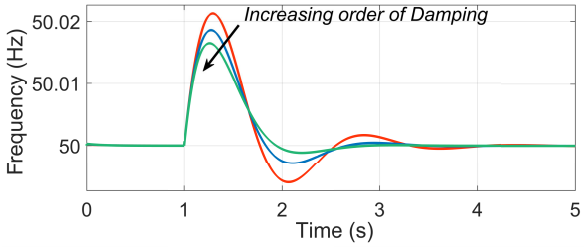

FIGURE 4. Frequency curve of VSG with variation in damping D_P.

C. VIRTUAL INERTIA'S IMPACT ON THE DYNAMIC PERFORMANCE OF VSG

Similarly, Effect of virtual inertia (J) on active power can be analyzed by using the derivative of transient performance parameters with respect to J.

From equation (11), we can see that,

$$\frac{dt_p}{dJ} > 0, \quad \frac{dt_s}{dJ} > 0 \quad \& \quad \frac{dM_p}{dJ} > 0 \tag{13}$$

By the analysis, the peak time of active power, settling time and peak overshoot, are increasing function with respect to J. Hence, peak time, settling time and peak overshoot of active power increases with increasing virtual inertia. The step response of active power with the variation in virtual inertia (J) is shown in Fig. 5.

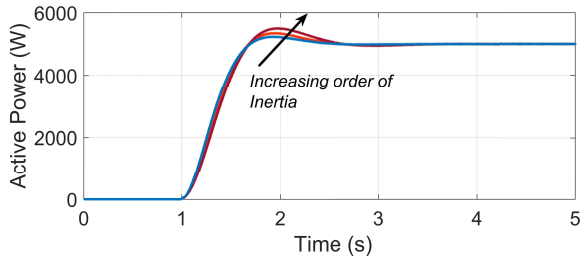

FIGURE 5. Active power response of VSG with variation in virtual inertia J.

Similarly, effect of virtual inertia J on frequency response can be analyzed using equation (8). Peak time & settling time of frequency response are increasing with respect to J. However, peak overshoot is decreasing with respect to virtual inertia J. Effect of variation of virtual inertia J on frequency response of VSG is shown in Fig. 6.

By analyzing the effect of inertia and damping on the dynamic behaviour of VSG, it is observed that both the parameters need to be adjusted for damping out the oscillations properly.

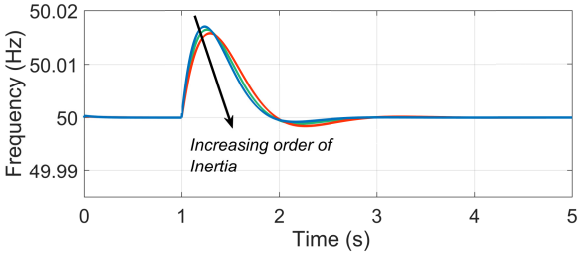

FIGURE 6. Frequency curve of VSG with variation in virtual inertia J.

V. ANALYSIS OF THE ENERGY STORAGE

From Eq.(10), Step response of active power is given by:

$$\hat{P_e} = \hat{P_m}[1 - \frac{e^{-\zeta\omega_N t}}{\sqrt{(1-\zeta^2)}} sin(\omega_d t + \phi)]$$

The $\hat{P_m}$ represents the step change in the reference value of active power, and the area confined between $\hat{P_m}$ and $\hat{P_e}$ denotes the energy consumed/supplied by the DC storage unit. Hence, the energy consumed/supplied by the storage segment is calculated as,

$$\begin{aligned} E(t) &= \int_0^t [\hat{P}_m - \hat{P}_e(t)]dt \\ &= \hat{P}_m \frac{e^{-\zeta\omega_N t}}{\omega_N}[\cos(\omega_d t + \phi) + \frac{\zeta}{\sqrt{1-\zeta^2}} \sin(\omega_d t + \phi)] \end{aligned} \tag{14}$$

The following section discusses, the energy absorbed by the storage segment for both critically damped and under-damped system.

Case I: For critically damped system ($\zeta = 1$)

Energy absorbed for critically damped system can be expressed as equation (15) by substituting $\zeta = 1$ in equation (14):

$$E(t) = \frac{\hat{P_m}}{\omega_N}[2 - 2e^{-\omega_N t} - \omega_N t e^{-\omega_N t}] \tag{15}$$

For critically damped system, total amount of energy that the storage segment needs to absorb during the disturbance in real power is computed by keeping t$\rightarrow\infty$.

$$E(\infty) = \frac{2\hat{P_m}}{\omega_N} \tag{16}$$

Fig. 7 shows the energy absorbed/supplied by the storage device in case of critically damped system for the step response of active power.

Case II: For under-damped system ($0 < \zeta < 1$)

Hence, total energy absorbed by the storage device until the active power reaches to equilibrium state for the very first time i.e. rise time, is derived by substituting $t = t_r$ in the above expression.

$$E(t_r) = \hat{P}_m \frac{e^{-\zeta\omega_N t_r}}{\omega_N}[\cos(\omega_d t_r + \phi)$$

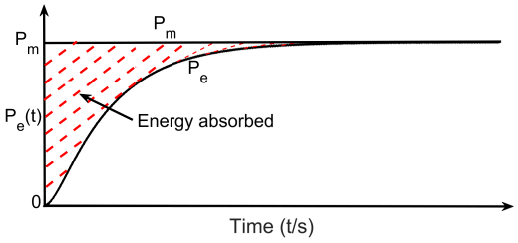

FIGURE 7. Active power of VSG for critically damped system.

$$+\frac{\zeta}{\sqrt{1-\zeta^2}}\sin(\omega_d t_r+\phi)] \tag{17}$$

Total Energy absorbed in case of under-damped system is calculated by substituting $t_r = (\pi - \phi)/\omega_d$ as,

$$E = \frac{\hat{P_m}}{\omega_N} e^{\frac{-\zeta(\pi-\phi)}{\sqrt{1-\zeta^2}}} \tag{18}$$

Equation (18) provides the energy required for sizing of the storage device for the under-damped scenario when the real power disturbances occur. Energy absorbed by the storage unit in case of under-damped system is shown by step response of active power in the Fig. 8.

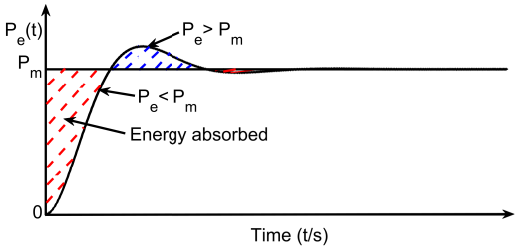

FIGURE 8. Active power of VSG for under-damped system.

According to the above analysis, there is no overshoot in the active power output when the system is critically damped, but the system responds slowly and requires more energy storage than an under-damped system does. So, there is a trade-off between under-damping and critically damping system while designing the energy storage. Therefore, to reduce the energy storage requirement, the design of the system needs to be slightly under-damped ($\zeta = 0.707$) with power oscillations kept within acceptable limits.

VI. PROPOSED FLEXIBLE VIRTUAL INERTIA AND DAMPING CONTROL

In this section, the proposed control algorithm is designed by using energy storage requirement and adaptive virtual inertia and damping. By using Eq. (14), energy of the storage unit is,

$$E(t) = \int_0^t [\hat{P}_m - \hat{P}_e(t)]dt$$

Using small signal perturbation,

$$\omega = \omega_n + \hat{\omega}, \quad \omega_0 = \omega_{0n} + \hat{\omega_0}, \quad E = E_0 + \hat{E} \tag{19a}$$

$$J = J_0 + \hat{J}, \quad D_P = D_{P0} + \hat{D_P} \tag{19b}$$

Using equation (19a)-(19b), derivative of E from equation (14) can be written as below:

$$\frac{d(\hat{E})}{dt} = \hat{P_m} - \hat{P_e}(t) \tag{20}$$

Energy stored by virtual rotor can be expressed as,

$$E = \frac{1}{2}J\omega^2 \tag{21}$$

$$\frac{dE}{dt} = \frac{d}{dt}(\frac{1}{2}J\omega^2) \tag{22}$$

From equation (20), the equation (22) can be rewritten as,

$$\frac{d\hat{E}}{dt} = J_0\omega_n\frac{d}{dt}\hat{\omega} + \frac{1}{2}\omega_n^2\frac{d\hat{J}}{dt} \tag{23}$$

Substituting the value of $\frac{d(\hat{E})}{dt}$ from equation (20) into equation (23) gives the expression as given in equation (24),

$$\hat{P_m} - \hat{P_e} = J_0\omega_n\frac{d}{dt}\hat{\omega} + \frac{1}{2}\omega_n^2\frac{d\hat{J}}{dt} \tag{24}$$

Applying perturbation in equation (2) we get,

$$(\hat{P_m} - \hat{P_e}) - D_P(\omega_0\hat{\omega}) = J\omega_0\frac{d\omega}{dt} \tag{25}$$

Substituting the value of $\hat{P_m} - \hat{P_e}$ from (24) into the equation (25), we get the relation as given in equation (26),

$$J_0\omega_n\frac{d\hat{\omega}}{dt} + \frac{1}{2}\omega_n^2\frac{d\hat{J}}{dt} - (D_{P0} + \hat{D_P})(\omega_{0n} + \hat{\omega_0})\hat{\omega} = (J_0 + \hat{J})(\omega_{0n} + \hat{\omega_0})\frac{d(\omega_n + \hat{\omega})}{dt} \tag{26}$$

Then by simplifying the equation (26) by neglecting the dc terms and product of the small variations, we get equation (27) as,

$$\frac{1}{2}\omega_{0n}^2\frac{d\hat{J}}{dt} = D_{P0}\omega_{0n}\hat{\omega} \tag{27}$$

Solving the equation (27), variable inertia is derived as given in the equation (28),

$$\hat{J} = \frac{2D_{P0}}{\omega_{0n}}\hat{\delta} \tag{28}$$

Since, damping ratio of the second order active power transfer function of equation (7) is $\zeta = \frac{D_P}{2J\omega_n}$. Hence, D_P can be rewritten as given in equation (29),

$$D_P = 2J\zeta\omega_N \tag{29}$$

Substituting the values of D_P and J from equation (19b) into (29) and ignoring the dc terms, expression for variable damping is derived as given in equation (30),

$$\hat{D_P} = 2\zeta(\hat{J}\omega_{N0} + J_0\hat{\omega_N}) \tag{30}$$

$$\text{where,} \quad \omega_{N0} = \sqrt{\frac{K}{J_0\omega_{0n}}} \tag{31}$$

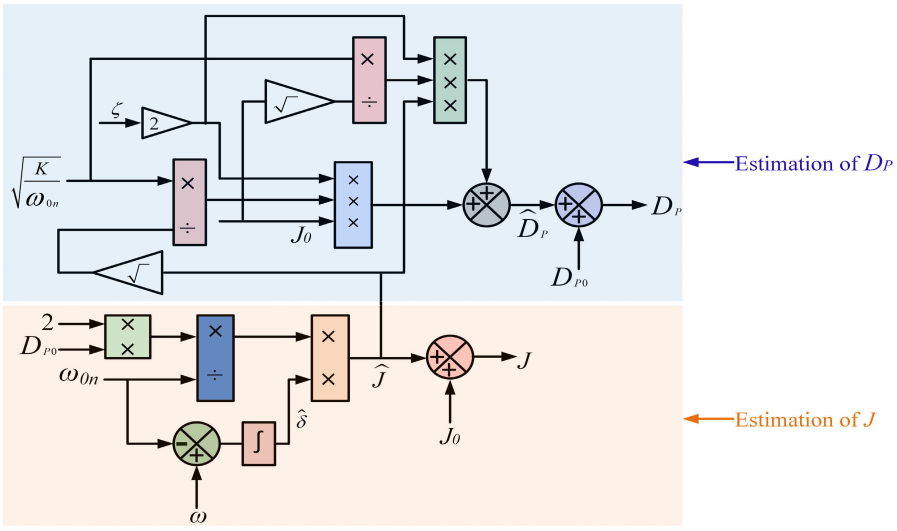

(a)

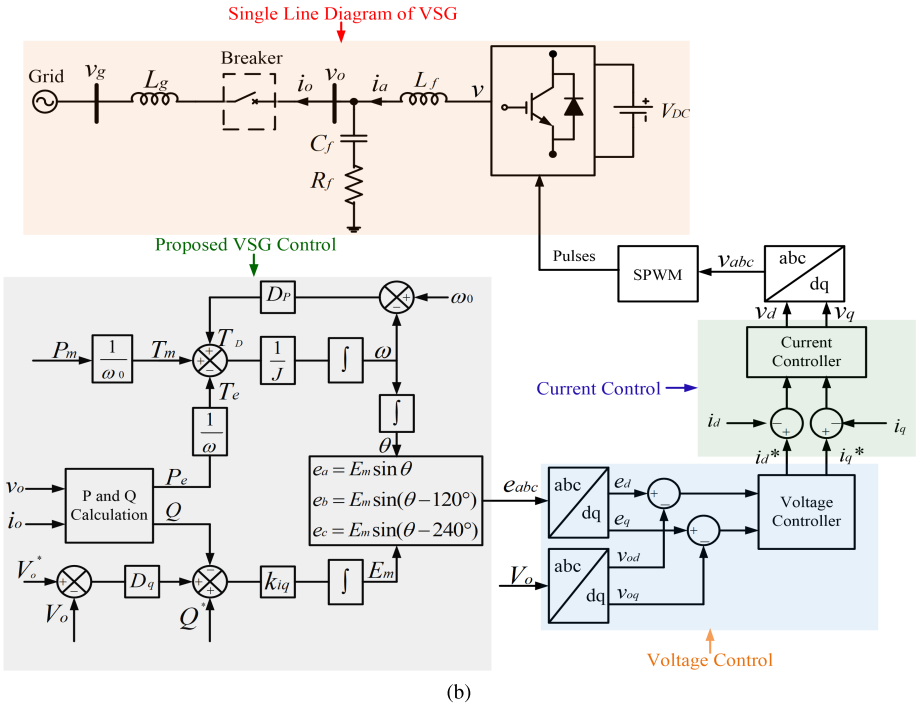

(b)

FIGURE 9. Proposed control method of VSG (a) Estimation of adaptive J and D_P (b) Complete VSG control algorithm.

From equation (28) and (30), the desired value of flexible virtual inertia and damping are calculated as,

$$J = J_0 + \hat{J}, \qquad D_P = D_{P0} + \hat{D}_P \tag{32}$$

where, J_0 and D_{P0} are steady state values of virtual inertia and virtual damping respectively. D_{P0} is determined based on the grid code. According to [8], 2% change in grid frequency causes 100% change in real power. J_0 is determined by putting D_{P0} into equation (9). Proposed control method for VSG is shown in Fig. 9. Flexible J and D_P values are updated according to Eqn.(32) as shown in Fig. 9 (a). Complete control algorithm of VSG is shown in Fig. 9 (b).

VII. SIMULATION RESULTS

The proposed control algorithm is simulated using MATLAB/simulink environment. Simulation parameters are shown in Appendix-A. At first, the proposed control algorithm is verified with the simulation results. Later, the proposed control strategy is compared with the adaptive J control [21] and Alternating J and D_P control [26] of VSG.

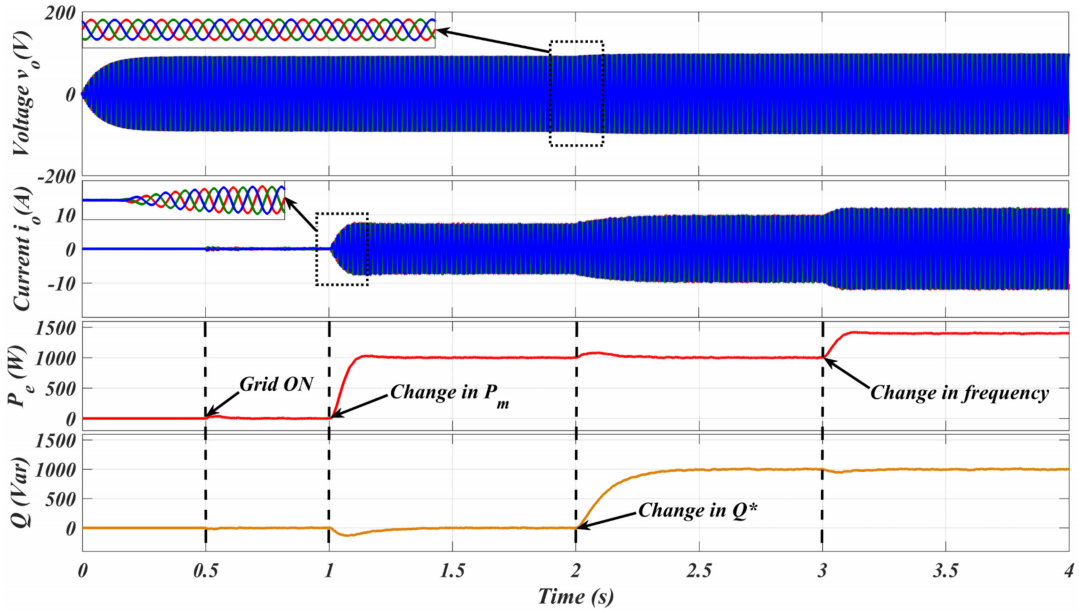

FIGURE 10. VSG response with the proposed control method.

A. SIMULATION RESULTS OF THE PROPOSED CONTROL ALGORITHM

The developed VSG control algorithm is tested for the synchronization, variation in reference active power, reference reactive power and grid frequency. Response of the VSG voltage v_o, current i_o, real power P_e and reactive power Q with proposed control method is shown in Fig. 10. Simulation results are explained in the following subsections.

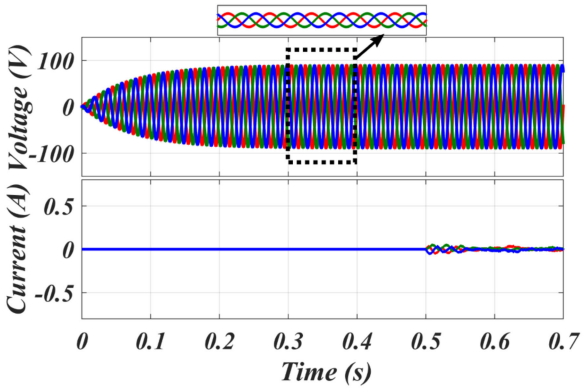

FIGURE 11. VSG voltage and current while grid connection.

1) SYNCHRONIZATION

From $t = 0$ seconds, as shown in Fig.11, VSG is working in islanded mode and maintains constant output voltage and frequency. At $t = 0.5$ seconds, circuit breaker is turned on and VSG is connected to the grid smoothly. So, there is no change in VSG output voltage and current before and after grid connection as shown in Fig. 11. At 1 s, the active power is changed from 0 to 1 kW. So, the current starts increasing at 1 s. as shown in Fig. 12.

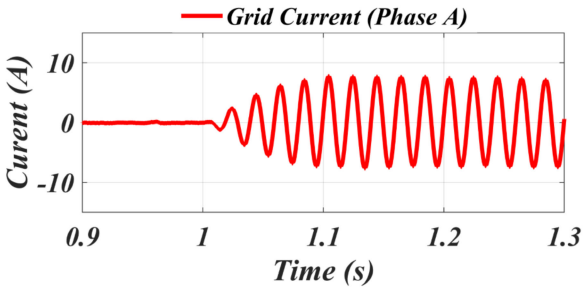

FIGURE 12. Grid current i_{oa} of proposed control.

The steady state current, voltage at power reference of 1 kW are shown in Fig. 13.

2) CHANGE IN REFERENCE ACTIVE POWER, REACTIVE POWER, AND GRID FREQUENCY

Initially, active and reactive power reference was set to zero i.e. $P_m = 0$ & $Q^* = 0$. At $t = 1$ seconds, active power reference P_m to the grid is changed from 0 to 1 kW. Active power P_e of VSG follows the reference power P_m with some oscillations and delay due to virtual damping and inertia as shown in Fig. 14. Hence, VSG fulfils the active power demand of the grid without affecting reactive power flow.

At $t = 2$ seconds, the reference reactive power Q^* is set to 1 kVar. So, VSG supplies 1 kVar reactive power to the grid as shown in Fig. 14. While, active power of VSG is observed to be almost no change.

At $t = 3$ seconds, grid frequency was decreased from its nominal value i.e. 50 Hz to 49.8 Hz. During this time, VSG supplies active power to the grid even the active power reference was not changed. Hence, VSG participates in frequency regulation process by supplying active power to

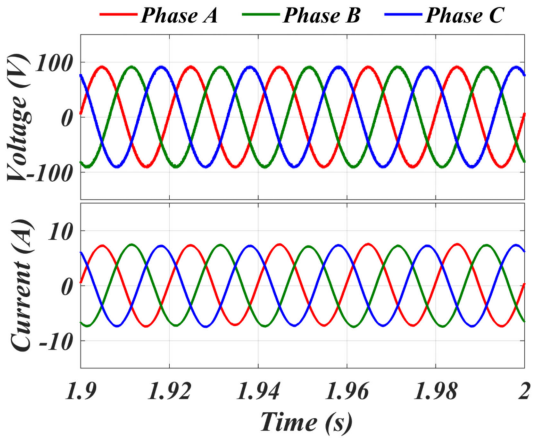

FIGURE 13. Output voltage and current of VSG with proposed method.

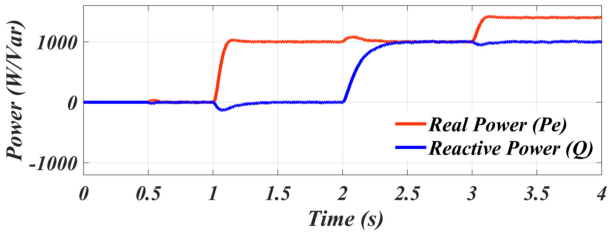

FIGURE 14. Variation in active power (P_e) and Reactive power (Q) with change in reference active power (P_m), reference reactive power (Q^*) and grid frequency ω_g.

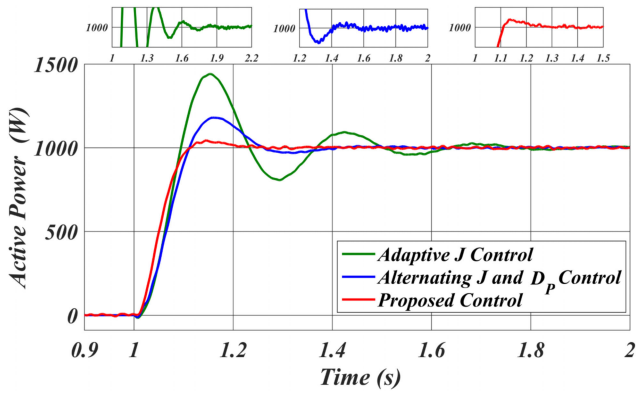

FIGURE 15. Output power of VSG.

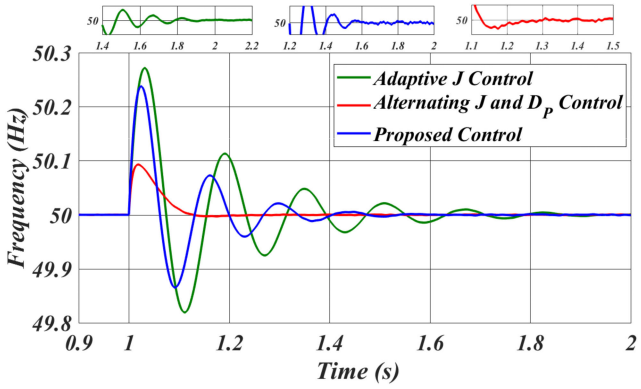

FIGURE 16. Output frequency of VSG.

the grid. Reactive power supplied by VSG does not change because, it is not dependent on frequency. Simulation was stopped at $t = 4$ seconds.

B. COMPARISON WITH THE ADAPTIVE J CONTROL AND ALTERNATING J AND D_P CONTROL

The results of the proposed control method is compared with the already existing adaptive J control [21] and alternating J and D_P control [26] and presented in Fig. (15-16). Fig. 15 presents the variation in active power for all three cases with the step change of 1 kW in reference active power. From Fig. 15, one can observe that, the proposed control method has shown less peak overshoot and less settling time. Fig. 16 presents the variation in frequency of the VSG for all three cases when there is a step change in reference active power. It is observed that proposed control method shows minimum frequency deviation from the steady state and shows the shortest settling time than other two adaptive control methods.

Fig. 15 demonstrates that adaptive J control has the maximum overshoot of 440 W and the longest settling time of 0.9 s. Comparing with the existing adaptive J control of VSG, alternating J and D_P control shows significant reduction in the overshoot and settling time with only 180 W overshoot and 0.6 s settling time. So, alternating J and D_P control method is effective in reducing the power fluctuations. However, the proposed adaptive control method shows the least overshoot of 40 W and settling time of 0.3 s as compared to other two methods. Hence, proposed control method gives the best active power response of VSG.

Also, the adaptive J control has larger frequency variation of 0.275 Hz and longer settling time of 0.9 s, while the proposed method is most effective in suppressing the frequency transients. Alternating J and D_P control reduces the frequency deviation to 0.24 Hz in comparison to adaptive J control of VSG. Settling time of frequency is also reduced to 0.6 s. Hence, frequency oscillations are reduced and frequency is restored quickly as compared to adaptive J control of VSG. In addition, with the proposed adaptive control method, frequency deviation is further reduced to 0.09 Hz as compared to the alternating J and D_P control of VSG. Settling time of frequency is further reduced to 0.3 s which, shows the effectiveness of proposed control method.

Comparison of the proposed control method with the existing adaptive control methods with respect to different parameters i.e. peak overshoot, settling time and energy supplied by the storage element is shown in Table 1. Comparison of the proposed method with the other two control methods considering the qualitative issues such as implementation complexity, size of the storage element etc. is presented in Table 2.

Since, the oscillations in the active power and frequency of VSG is minimum in the proposed flexible method as compared to the other two adaptive control methods, the

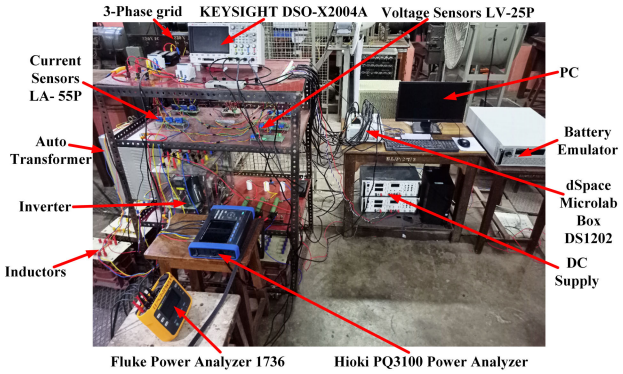

FIGURE 17. VSG hardware prototype.

energy absorbed/supplied by the storage element is minimum in the proposed method as shown in Table 1. As a result, the size of the storage element is reduced.

VIII. EXPERIMENTAL RESULTS

A. EXPERIMENTAL RESULTS WITH PROPOSED ALGORITHM

A prototype of VSG system is prepared in the laboratory for the verification of the proposed control algorithm as shown in Fig. 17. Three-phase VSG prototype consists of interfacing inductor, three-phase transformer, inverter, and three phase grid, voltage sensors (LV25-P), current sensors (LA55-P). Power system analyzer (Fluke-1736 Power Logger) is used to record the steady-state output of the VSG system. The transient behaviour of the VSG is recorded using digital oscilloscope (KEYSIGHT infiniiVision DSOX2004A). Experimental parameters are shown in Appendix-B. The experimental results of the proposed VSG are presented in this section to show its superiority for both steady state and dynamic conditions.

1) SYNCHRONIZATION

Initially, VSG is working in islanded mode. For grid connection of VSG, synchronization control is activated to synchronize the output voltage of VSG with the grid voltage.

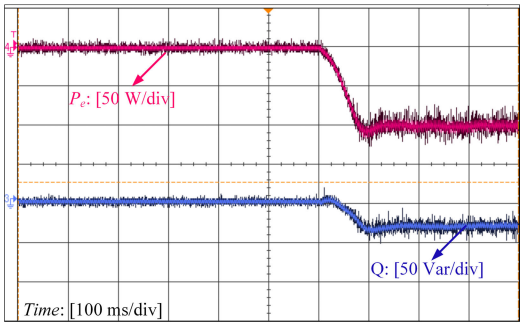

FIGURE 18. Active power P_e and reactive power Q of VSG after grid connection.

After synchronization, VSG is connected to the grid and because of variation in grid frequency and voltage amplitude, VSG exchanges some amount of active and reactive power with the grid as shown in Fig. 18. At this instant, the grid frequency is more than 50 Hz. Hence, VSG absorbs the active power from the grid, as shown in Fig. 18.

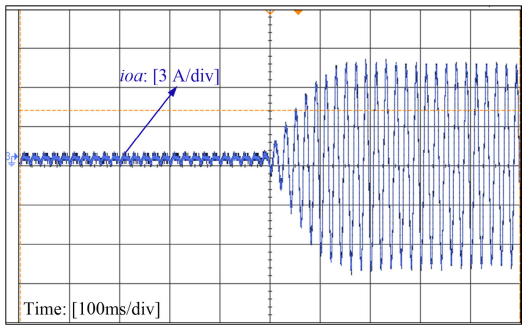

FIGURE 19. Grid current waveform with proposed method.

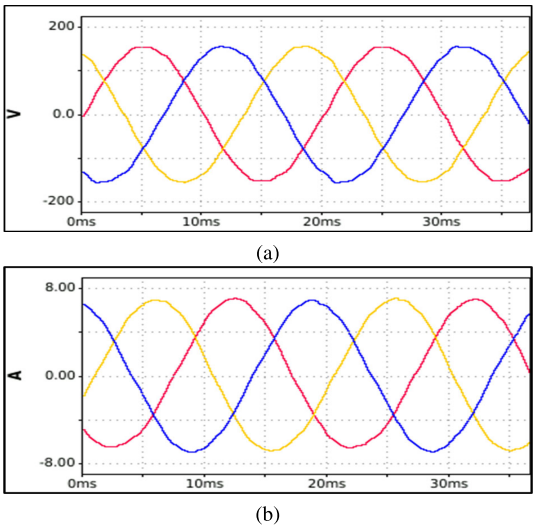

FIGURE 20. Output voltage and current waveforms of VSG (a) v_{oab}, v_{obc} and v_{oca} (b) i_{oa}, i_{ob} and i_{oc}.

The VSG output current/grid current i_{oa} with proposed method when output power P_e changes from 0 to 1 kW is shown in Fig.19. Three phase line voltages and current waveforms of VSG after it reaches to steady state are shown in Fig. 20.

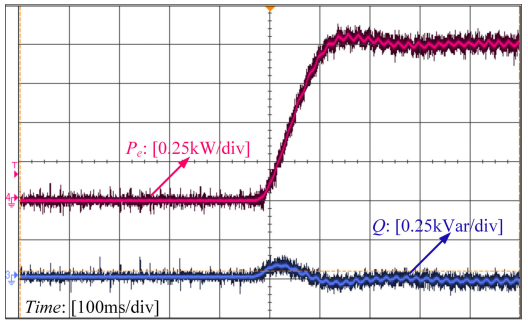

FIGURE 21. Change in active power P_e with the reference active power P_m.

TABLE 1. Comparison of proposed control with existing literature.

	Active Power		Frequency		Energy supplied
	Overshoot	Settling Time	Overshoot	Settling Time	
Adaptive J Control [21]	440 W	0.9 s	0.275 Hz	0.9 s	60 *Joule*
Alternating J and D_p Control [26]	180 W	0.6 s	0.24 Hz	0.6 s	56 *Joule*
Proposed Control	40 W	0.3 s	0.09 Hz	0.3 s	47 *Joule*

TABLE 2. Qualitative comparison of proposed control with existing literature.

	Implementation	Storage Size
Adaptive J Control [21]	Complex	Big
Alternating J and D_p Control [26]	More complex	Medium
Proposed Control	Less complex	Small

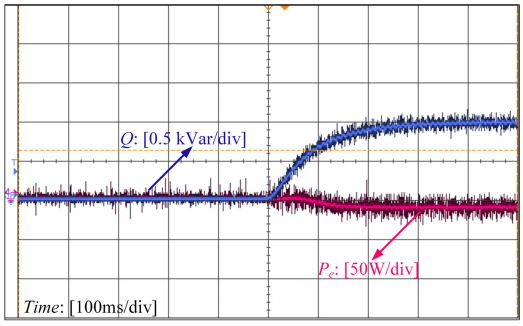

FIGURE 22. Change in reactive power Q with the reference reactive power Q^*.

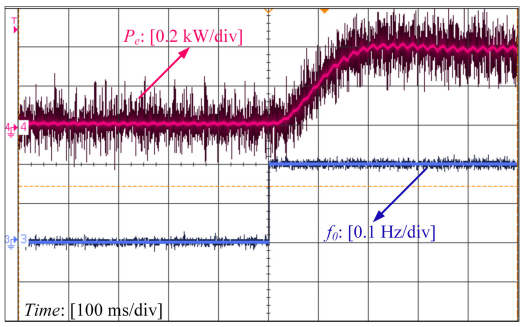

FIGURE 23. Change in active power P_e with VSG reference frequency.

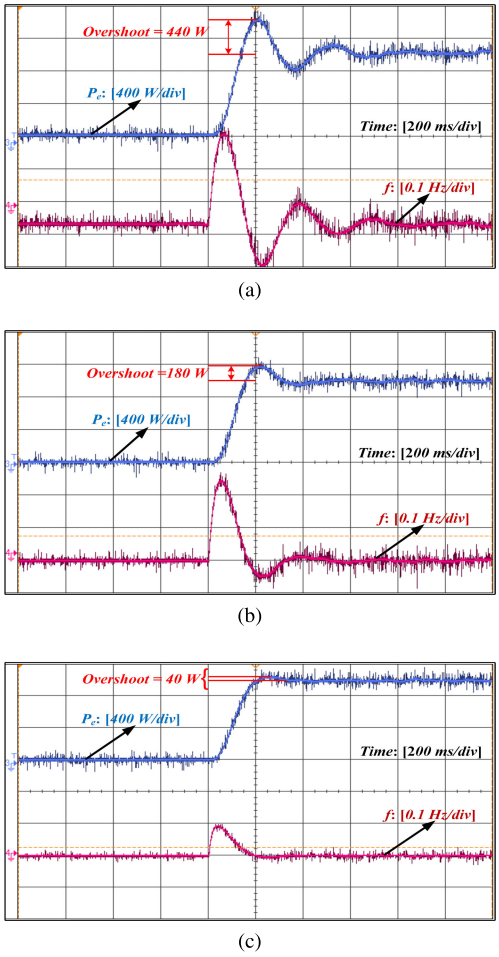

FIGURE 24. VSG output power and frequency response for a sudden change in the active power reference for (a) adaptive J control [21] (b) alternating J and D_P control [26] (c) proposed adaptive control.

Then, VSG is tested for its dynamic performance by changing its reference active and reactive powers and changing the VSG reference frequency, as discussed in the next subsection.

2) CHANGE IN REFERENCE ACTIVE POWER (P_M), REFERENCE REACTIVE POWER (Q^*) AND REFERENCE FREQUENCY (ω_0)

Initially, active power reference P_m to the grid is increased from 0 to 1 kW as depicted in Fig. 21, the active power exchange between VSG and grid starts occurring and there is no change in reactive power.

Now, reactive power reference Q^* to the grid is changed from 0 to 1 kVar assuming that there is no variation in active power reference, and frequency. VSG quickly supplies the reactive power Q according to the reference reactive power command as shown in Fig. 22.

The VSG is verified for the frequency regulation by changing the VSG reference frequency ω_0 (f_0 in Hz). VSG performs the frequency regulation by supplying or absorbing the real power to/from the grid. As the grid frequency can't be changed, the change in frequency is emulated by changing the VSG reference frequency. Variation of real power generated from VSG, when reference frequency f_0 is increased by 0.2 Hz, is shown in Fig. 23.

B. COMPARISON OF THE PROPOSED ADAPTIVE CONTROL WITH ADAPTIVE J CONTROL AND ALTERNATING J AND D_P CONTROL

VSG is tested with all three control methods i.e. adaptive J control [21], alternating J and D_P control [26] and proposed adaptive control and results are compared as shown in Fig. 24.

The dynamic response of the VSG active power P_e and VSG frequency ω (f in Hz) are recorded for step change of a 1 kW in reference active power. Fig. 24 (a), (b) and (c) shows the step response of power and frequency with adaptive J control, alternating J and D_P control and the proposed flexible inertia and damping control.

From Fig. 24, it is observed that experimental results validate the superiority of the proposed control method in terms of the reduced size of the storage device and less peak overshoot, less settling time in active power and frequency response as compared to the adaptive J control and alternating J and D_P control of VSG.

IX. CONCLUSION

Initially, the effect of variation of inertia and damping on VSG active power and frequency has been analyzed and it was established that frequency and active power oscillations can be vanquished by a bigger damping coefficient and a bigger inertia can take care of the rate of change of frequency as well as the oscillations in the active power. Further, it is concluded that there is a need to adjust both virtual inertia and damping together to improve the transient response of VSG active power loop. Energy absorbed/supplied by the storage unit was analyzed for both critically damped and under-damped system and observed that for an under-damped system, the energy storage requirement is lesser as compared to critically damped system. So, damping ratio and parameters of the VSG active power loop should be chosen to achieve under-damped response to reduce the energy storage requirements.

A flexible virtual inertia and damping control strategy for VSG for optimizing the energy storage was proposed in this paper. Proposed scheme was simulated in MATLAB/Simulink platform and also verified on a developed VSG experimental setup. Experimental results of the proposed control method was compared with the adaptive J control and alternating J and D_P control of VSG for a sudden change in the active power reference. Active power of VSG with the proposed control method have the best performance with 40 Watts overshoot and settling time of 0.3 seconds. In addition, VSG frequency shows best response with the proposed control method having least settling time of 0.3 seconds and overshoot of 0.09 Hz. Energy supplied by the storage unit with the proposed control method is also minimum and around 47 *Joule*. Hence, the proposed control method utilizes minimum energy storage and significantly reduces the output frequency deviation and settling time as compared to the other two methods. Further, active power oscillations were also reduced compared to other two control methods while reducing the settling time as well. Future research can be done for the multi-VSG system with the proposed adaptive control. Moreover, adaptive control of VSG under distorted grid condition can also be explored.

APPENDIX A
SIMULATION PARAMETERS

DC voltage: 220 V; 3-ϕ ac voltage: 110 V, 50 Hz; interfacing inductance (L_f): 3.5 mH; steady state virtual inertia (J_0): 0.1 kgm^2; steady state virtual damping (D_{P0}): 5.

APPENDIX B
EXPERIMENTAL PARAMETERS

DC voltage: 220 V, 3-ϕ ac voltage: 110 V, 50 Hz; interfacing inductance (L_f): 3.5 mH; steady state virtual inertia (J_0): 0.1 kgm^2; steady state virtual damping (D_{P0}): 5.

REFERENCES

[1] M. S. Mahmoud, *Microgrid: Advanced Control Methods and Renewable Energy System Integration*. Amsterdam, The Netherlands: Elsevier, 2017.

[2] Q.-C. Zhong and T. Hornik, *Control of Power Inverters in Renewable Energy and Smart Grid Integration*. Hoboken, NJ, USA: Wiley, 2013.

[3] Z.-S. Zhang, Y.-Z. Sun, J. Lin, and G.-J. Li, "Coordinated frequency regulation by doubly fed induction generator-based wind power plants," *IET Renew. Power Gener.*, vol. 6, no. 1, pp. 38–47, Jan. 2012.

[4] M. F. M. Arani and E. F. El-Saadany, "Implementing virtual inertia in DFIG-based wind power generation," *IEEE Trans. Power Syst.*, vol. 28, no. 2, pp. 1373–1384, May 2013.

[5] Q.-C. Zhong and G. Weiss, "Static synchronous generators for distributed generation and renewable energy," in *Proc. IEEE/PES Power Syst. Conf. Expo.*, Mar. 2009, pp. 1–6.

[6] T. Shintai, Y. Miura, and T. Ise, "Oscillation damping of a distributed generator using a virtual synchronous generator," *IEEE Trans. Power Del.*, vol. 29, no. 2, pp. 668–676, Apr. 2014.

[7] S. D'Arco and J. A. Suul, "Equivalence of virtual synchronous machines and frequency-droops for converter-based microgrids," *IEEE Trans. Smart Grid*, vol. 5, no. 1, pp. 394–395, Jan. 2014.

[8] K. M. Cheema, "A comprehensive review of virtual synchronous generator," *Int. J. Electr. Power Energy Syst.*, vol. 120, Sep. 2020, Art. no. 106006.

[9] Q.-C. Zhong and G. Weiss, "Synchronverters: Inverters that mimic synchronous generators," *IEEE Trans. Ind. Electron.*, vol. 58, no. 4, pp. 1259–1267, Apr. 2011.

[10] M. M. Islam, K. M. Muttaqi, D. Sutanto, M. M. Rahman, and O. Alonso, "Design of a controller for grid forming inverter-based power generation systems," *IEEE Access*, vol. 11, pp. 55755–55770, 2023.

[11] V. L. Srinivas, B. Singh, and S. Mishra, "Seamless mode transition technique for virtual synchronous generators and method thereof," *IEEE Trans. Ind. Informat.*, vol. 16, no. 8, pp. 5254–5266, Aug. 2020.

[12] M. Ashabani and J. Jung, "Synchronous voltage controllers: Voltage-based emulation of synchronous machines for the integration of renewable energy sources," *IEEE Access*, vol. 8, pp. 49497–49508, 2020.

[13] J. L. Rodríguez-Amenedo, S. A. Gómez, M. Zubiaga, P. Izurza-Moreno, J. Arza, and J. D. Fernández, "Grid-forming control of voltage source converters based on the virtual-flux orientation," *IEEE Access*, vol. 11, pp. 10254–10274, 2023.

[14] P. Utkarsha and N. K. S. Naidu, "Virtual synchronous machine based electric vehicle charger for meeting ancillary services," in *Proc. IEEE Transp. Electrific. Conf. (ITEC-India)*, Bengaluru, India, Dec. 2019, pp. 1–6.

[15] H. Wu, X. Ruan, D. Yang, X. Chen, W. Zhao, Z. Lv, and Q. Zhong, "Small-signal modeling and parameters design for virtual synchronous generators," *IEEE Trans. Ind. Electron.*, vol. 63, no. 7, pp. 4292–4303, Jul. 2016.

[16] M. Schweizer, S. Almér, S. Pettersson, A. Merkert, V. Bergemann, and L. Harnefors, "Grid-forming vector current control," *IEEE Trans. Power Electron.*, vol. 37, no. 11, pp. 13091–13106, Nov. 2022.
[17] M. Li, Y. Wang, Y. Liu, N. Xu, S. Shu, and W. Lei, "Enhanced power decoupling strategy for virtual synchronous generator," *IEEE Access*, vol. 8, pp. 73601–73613, 2020.
[18] K. Li, P. Cheng, L. Wang, X. Tian, J. Ma, and L. Jia, "Improved active power control of virtual synchronous generator for enhancing transient stability," *IET Power Electron.*, vol. 16, no. 1, pp. 157–167, Aug. 2022.
[19] N. Xu, Y. Wang, M. Li, W. Wang, N. Wang, and J. Li, "An optimal control method of virtual angular acceleration to improve transient response based on virtual synchronous generator," in *Proc. IEEE 3rd Int. Future Energy Electron. Conf. ECCE Asia (IFEEC-ECCE Asia)*, Jun. 2017, pp. 1559–1563.
[20] Y. Xiang-zhen, S. Jian-hui, D. Ming, L. Jin-wei, and D. Yan, "Control strategy for virtual synchronous generator in microgrid," in *Proc. 4th Int. Conf. Electric Utility Deregulation Restructuring Power Technol. (DRPT)*, Jul. 2011, pp. 1633–1637.
[21] J. Alipoor, Y. Miura, and T. Ise, "Power system stabilization using virtual synchronous generator with alternating moment of inertia," *IEEE J. Emerg. Sel. Topics Power Electron.*, vol. 3, no. 2, pp. 451–458, Jun. 2015.
[22] S. Wang, R. Qi, and Y. Li, "Fuzzy control scheme of virtual inertia for synchronverter in micro-grid," in *Proc. 21st Int. Conf. Electr. Mach. Syst. (ICEMS)*, Oct. 2018, pp. 2028–2032.
[23] T. Zheng, L. Chen, R. Wang, C. Li, and S. Mei, "Adaptive damping control strategy of virtual synchronous generator for frequency oscillation suppression," in *Proc. 12th IET Int. Conf. AC DC Power Transmiss. (ACDC)*, May 2016, pp. 1–5.
[24] M. A. L. Torres, L. A. C. Lopes, L. A. T. Morán, and J. R. C. Espinoza, "Self-tuning virtual synchronous machine: A control strategy for energy storage systems to support dynamic frequency control," *IEEE Trans. Energy Convers.*, vol. 29, no. 4, pp. 833–840, Dec. 2014.
[25] R. Shi, X. Zhang, C. Hu, H. Xu, J. Gu, and W. Cao, "Self-tuning virtual synchronous generator control for improving frequency stability in autonomous photovoltaic-diesel microgrids," *J. Modern Power Syst. Clean Energy*, vol. 6, no. 3, pp. 482–494, May 2018.
[26] F. Wang, L. Zhang, X. Feng, and H. Guo, "An adaptive control strategy for virtual synchronous generator," *IEEE Trans. Ind. Appl.*, vol. 54, no. 5, pp. 5124–5133, Sep. 2018.
[27] X. Zhang, F. Mao, H. Xu, F. Liu, and M. Li, "An optimal coordination control strategy of micro-grid inverter and energy storage based on variable virtual inertia and damping of vsg," *Chin. J. Electr. Eng.*, vol. 3, no. 3, pp. 25–33, Dec. 2017.
[28] A. S. Mir and N. Senroy, "Self-tuning neural predictive control scheme for ultrabattery to emulate a virtual synchronous machine in autonomous power systems," *IEEE Trans. Neural Netw. Learn. Syst.*, vol. 31, no. 1, pp. 136–147, Jan. 2020.
[29] F. Yao, J. Zhao, X. Li, L. Mao, and K. Qu, "RBF neural network based virtual synchronous generator control with improved frequency stability," *IEEE Trans. Ind. Informat.*, vol. 17, no. 6, pp. 4014–4024, Jun. 2021.
[30] Z. Wang, Y. Yu, W. Gao, M. Davari, and C. Deng, "Adaptive, optimal, virtual synchronous generator control of three-phase grid-connected inverters under different grid conditions—An adaptive dynamic programming approach," *IEEE Trans. Ind. Informat.*, vol. 18, no. 11, pp. 7388–7399, Nov. 2022.
[31] M. Yang, Y. Wang, X. Xiao, and Y. Li, "A robust damping control for virtual synchronous generators based on energy reshaping," *IEEE Trans. Energy Convers.*, vol. 38, no. 3, pp. 2146–2159, Sep. 2023.

PRATEEK UTKARSHA (Graduate Student Member, IEEE) received the B.E. degree in electrical engineering and the M.E. degree in power systems from the University Institute of Technology (Rajiv Gandhi Technological University), Bhopal, Madhya Pradesh, India, in 2012 and 2017, respectively. He is currently pursuing the Ph.D. degree with the Department of Electrical Engineering, Indian Institute of Technology (BHU) Varanasi, Varanasi, India.

His research interests include renewable energy generation systems, power quality, grid forming inverters, and grid connected photovoltaic (PV) systems.

N. K. SWAMI NAIDU received the B.Tech. degree in electrical and electronics engineering from Jawaharlal Nehru Technological University (JNTU), Hyderabad, India, in 2007, the M.Tech. degree in power electronics and drives from the National Institute of Technology, Kurukshetra, India, in 2009, and the Ph.D. degree from the Electrical Engineering Department, Indian Institute of Technology Delhi, New Delhi, India, in 2015.

He is currently an Assistant Professor with the Department of Electrical Engineering, Indian Institute of Technology (BHU) Varanasi, Varanasi, India. His research interests include power electronics, wind energy conversion systems, power quality, and microgrid-based power systems.

BATTA SIVAPRASAD was born in Andhra Pradesh, India, in 1992. He received the B.Tech. and M.Tech. degrees in electrical engineering from Jawaharlal Nehru Technological University (JNTU) Kakinada, in 2012 and 2016, respectively. He is currently pursuing the Ph.D. degree with the Department of Electrical Engineering, Indian Institute of Technology (BHU) Varanasi, Varanasi, India.

His research interests include grid forming inverters and their ancillary services, renewable energy sources, and energy storage systems.

KUMAR ABHISHEK SINGH received the B.E. degree in electrical engineering from the Bhilai Institute of Technology, Durg, Chhattisgarh, India, in 2015, and the M.Tech. degree in electrical machines and drives and the Ph.D. degree in electrical engineering from the Indian Institute of Technology (BHU) Varanasi, Varanasi, India, in 2017 and 2022, respectively.

His research interests include electric machine drives, renewable energy integration in DC microgrid, wind energy conversion systems, solar and wind hybrid energy systems, and power electronic converters.